Journal of Photochemistry and Photobiology A: Chemistry 209 (2010) 203–209

Contents lists available at ScienceDirect

Journal of Photochemistry and Photobiology A: Chemistry

journal homepage: www.elsevier.com/locate/jphotochem

Synthesis, characterization, and study of the photophysics and photocatalytic properties of the photoinitiated electron collector $[\{(phen)_2Ru(dpp)\}_2RhBr_2](PF_6)_5$

Travis A. White, Krishnan Rangan, Karen J. Brewer*

Department of Chemistry, Virginia Polytechnic and State University, Blacksburg, VA 24060-0212, United States

ARTICLE INFO

Article history:
Received 7 September 2009
Received in revised form
10 November 2009
Accepted 23 November 2009
Available online 26 November 2009

Keywords:
Photocatalysis
Hydrogen production
Mixed-metal
Supramolecular
Bridging ligand
Metal-to-ligand charge transfer
Metal-to-metal charge transfer
Multi-electron photochemistry
1,10-Phenanthroline

ABSTRACT

The heterometallic photoinitiated electron collector $[\{(phen)_2Ru(dpp)\}_2RhBr_2](PF_6)_5$ (phen = 1,10-phenanthroline, dpp = 2,3-bis(2-pyridyl)pyrazine) has been synthesized and studied by spectroscopic, photophysical, electrochemical, and photochemical techniques. Substitution of chloride with bromide in the previously reported $[\{(phen)_2Ru(dpp)\}_2RhCl_2](PF_6)_5$ complex presents a new photoinitiated electron collector which can assist in understanding the functioning of our supramolecular systems $[\{(TL)_2Ru(BL)\}_2RhX_2](PF_6)_5$ (TL = terminal ligand, BL = bridging ligand, X = halide) in the photoinitiated electron collection and generation of hydrogen through the reduction of water and a detailed comparison is presented. Both the bromide and chloride analogues of these supramolecular complexes contain low energy, emissive metal-to-ligand charge transfer (^{3}MLCT) excited states that populate lower lying metal-to-metal charge transfer (^{3}MMCT) excited states. The electrochemistry of these complexes showed an impact on the reduction of the central Rh^{III} upon halide substitution with the bromide analogue $[(phen)_2Ru(dpp)\}_2RhBr_2](PF_6)_5$ having a slightly lower reduction potential than the corresponding chloride counterpart. The more positive reduction of Rh^{III} to generate the Rh^{I} species in the bromide analogue impacts the photocatalytic properties upon photolysis in the presence of a sacrificial electron donor. The trimetallic complex $[\{(phen)_2Ru(dpp)\}_2RhBr_2](PF_6)_5$ generates hydrogen through the reduction of water with higher yields than the chloride $[\{(phen)_2Ru(dpp)\}_2RhCl_2](PF_6)_5$ analogue under the same conditions. Despite the longer lived ^{3}MLCT state of both $[(TL)_2Ru(dpp)]^{2+}$ and $[\{(TL)_2Ru\}_2(dpp)]^{4+}$ when TL = phen vs. bpy (bpy = 2,2′-bipyridine), the phen trimetallics with X = Cl^- or Br^- do not display longer lived ^{3}MLCT states and show lower H_2 yields than the analogous bpy trimetallic systems.

1. Introduction

Supramolecular complexes functioning as photoinitiated electron collectors are capable of being designed as multi-electron photocatalysts [1]. In many cases, photoinitiated electron collectors incorporate metal-based light absorbers containing polypyridyl terminal ligands, polyazine bridging ligands, and electron collecting units [2–5]. Variation of the molecular components within these complexes can influence spectroscopic, photophysical and electrochemical properties, as well as the photocatalytic properties. Polypyridyl terminal ligands and polyazine bridging ligands are shown in Fig. 1. The Brewer group reported the first photochemical molecular device that functions as a photoinitiated electron collector [6]. The trimetallic complex $[\{(bpy)_2Ru(dpb)\}_2IrCl_2](PF_6)_5$ (bpy = 2,2′-bipyridine, dpb = 2,3-bis(2-pyridyl)benzoquinoxaline) has been shown to collect electrons in the bridging ligand π* LUMO upon photoexcitation. MacDonnell and Campagna [7,8] reported bimetallic complexes $[(phen)_2Ru(BL)Ru(phen)_2](PF_6)_4$ (BL = 9,11,20,22-tetraazatetrapyrido[3,2-a:2′3′-c:3″,2″-1:2‴,3‴-n]pentacene (tatpp) or 9,11,20,22-tetraazatetrapyrido[3,2-a:2′3′-c:3″,2″-1:2‴,3‴-n]pentacene-10,21-quinone (tatpq)) that are capable of storing up to two or four electrons in the bridging ligand π* LUMO, respectively. The first functioning photoinitiated electron collector $[\{(bpy)_2Ru(dpp)\}_2RhCl_2](PF_6)_5$ (dpp = 2,3-bis(2-pyridyl)pyrazine) to collect electrons at a reactive metal center while remaining intact following reduction was reported by Brewer [9]. Following photoexcitation, reduction of the metal center and subsequent halide loss generates the square planar Rh^{I} species. Enhanced photocatalytic activity was observed upon varying the halide from chloride to bromide in the trimetallic complex $[\{(bpy)_2Ru(dpp)\}_2RhBr_2](PF_6)_5$ for the generation of H_2 from water in the presence of an electron donor [10]. The phen analogue $[\{(phen)_2Ru(dpp)\}_2RhCl_2](PF_6)_5$ of the bpy trimetallic complex

* Corresponding author. Tel.: +1 540 231 6579; fax: +1 540 231 3255.
E-mail address: kbrewer@vt.edu (K.J. Brewer).

1010-6030/$ – see front matter © 2009 Published by Elsevier B.V.
doi:10.1016/j.jphotochem.2009.11.015

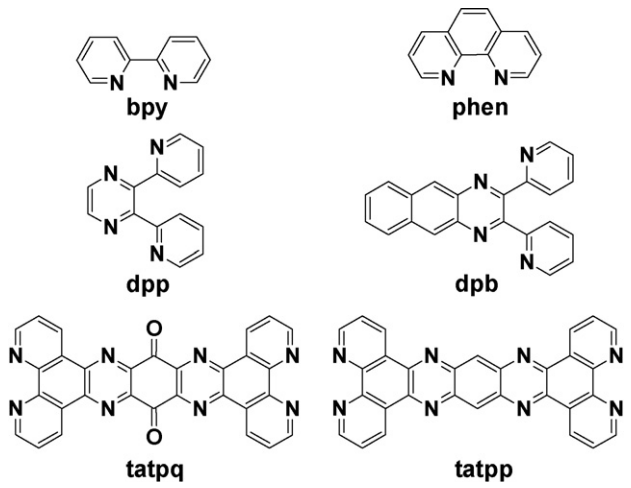

Fig. 1. Terminal and bridging ligands. bpy = 2,2′-bipyridine; phen = 1,10-phenanthroline; dpp = 2,3-bis(2-pyridyl)pyrazine; dpb = 2,3-bis(2-pyridyl)benzoquinoxaline; tatpq = 9,11,20,22-tetraazatetrapyrido[3,2-a:2′3′-c:3″,2″-1:2‴,3‴-n]pentacene-10,21-quinone; tatpp = 9,11,20,22-tetraazatetrapyrido[3,2-a:2′3′-c:3″,2″-1:2‴,3‴-n]pentacene.

has shown to function as a photoinitiated electron collector as well, indicating that other polypyridyl terminal ligands are capable of being used [11].

Reported herein are the spectroscopic, photophysical, electrochemical, and photochemical properties of the new photoinitiated electron collector $[\{(phen)_2Ru(dpp)\}_2RhBr_2](PF_6)_5$ with a detailed comparison of the phen vs. bpy and bromide vs. chloride trimetallic systems. This Ru,Rh,Ru trimetallic complex is able to photocatalytically reduce water to generate hydrogen while still remaining intact after successive catalytic cycles.

2. Experimental

2.1. Materials

All solvents and chemicals were used as received unless otherwise stated. The complexes $[\{(bpy)_2Ru(dpp)\}_2RhCl_2](PF_6)_5$ [9], $[\{(bpy)_2Ru(dpp)\}_2RhBr_2](PF_6)_5$ [10] and $[\{(phen)_2Ru(dpp)\}_2RhCl_2](PF_6)_5$ [11] were prepared as previously described.

2.2. Synthesis of $[\{(phen)_2Ru(dpp)\}_2RhBr_2](PF_6)_5$

The precursor complex $[(phen)_2Ru(dpp)](PF_6)_2$ was synthesized by modification of a previously reported method [12,13]. Using column chromatography, purification was achieved with methanol deactivated alumina as the stationary phase and 2:3 acetonitrile:toluene as the mobile phase. ESI-MS: $[M-PF_6]^+$, $m/z = 841$. The title complex $[\{(phen)_2Ru(dpp)\}_2RhBr_2](PF_6)_5$ was synthesized by heating at reflux $[(phen)_2Ru(dpp)](PF_6)_2$ (0.60 g, 0.60 mmol) and $RhBr_3{\cdot}3H_2O$ (0.14 g, 0.35 mmol) in a 2:1 $EtOH/H_2O$ solution (40 mL) for 1 h. The sample solution was allowed to cool before adding dropwise to an aqueous NH_4PF_6 solution (100 mL) to induce precipitation as a PF_6^- salt. The sample was filtered, washed with water, hot ethanol, diethyl ether and dried under vacuum in a desiccator overnight. Enhanced purity of $[\{(phen)_2Ru(dpp)\}_2RhBr_2](PF_6)_5$ was achieved by recrystallization of the sample from hot ethanol to obtain a dark maroon solid (0.56 g, 0.23 mmol, yield = 73%). Electronic absorption spectroscopy in CH_3CN, λ_{max} ($\varepsilon \times 10^{-4}\,M^{-1}\,cm^{-1}$): 224 nm (15.2), 262 nm (15.9), 346 nm (3.9), 418 nm (2.3), 520 nm (2.6). ESI-MS: $[M-PF_6]^+$, $m/z = 2235$.

2.3. Electronic absorption spectroscopy

The electronic absorption spectra were obtained using a Hewlett Packard 8452A diode array spectrophotometer. The wavelength range of measurement was 190–820 nm with a sampling interval of 2 nm and an integration time of 0.5 s. The samples were measured in UV-grade acetonitrile at room temperature using a 1 cm path length quartz cuvette (Starna Cells, Inc., Atascadero, CA). The extinction coefficient measurements were performed in triplicate.

2.4. Luminescence spectroscopy

The room temperature steady state emission spectra were collected in degassed UV-grade acetonitrile using a 1 cm path length quartz cuvette. The instrument used to record the spectra was a QuantaMaster Model QM-200-45E fluorimeter from Photon Technologies International, Inc. The source of excitation was a water-cooled 150 W Xenon arc lamp, with the corresponding emission collected at a 90° angle using a thermoelectrically cooled Hamamatsu 1527 photomultiplier tube operating in photon counting mode with 0.25 nm resolution. The emission quantum yields were measured against $[Os(bpy)_3]^{2+}$ ($\Phi^{em} = 4.62 \times 10^{-3}$) with all samples studied using the same instrument settings [14]. The 77 K emission spectra were obtained using a 4:1 ethanol/methanol solution submerged in liquid N_2 in a finger dewar to form a rigid glass matrix. The emission spectra were corrected for PMT response.

2.5. Excited state lifetime measurements

The excited state lifetimes were measured using a Photon Technologies International, Inc. PL-2300 nitrogen laser with an attached PL-201 tunable dye laser as the source of excitation. The dye used was Coumarin 500 and the excitation monochromator was set to 520 nm. The emission was detected at a 90° angle from the excitation source after passing through an emission monochromator set to 746 nm using a Hamamatsu R928 photomultiplier tube operating in direct analog mode. The signal was recorded using a LeCroy 9361 oscilloscope which averaged the results of 300 sweeps. All complexes were studied with the same instrument settings.

2.6. Electrochemistry

Cyclic voltammograms were obtained using a Bioanalytical Systems (BAS) Epsilon electrochemical analyzer with a three electrode, single compartment cell. The supporting electrolyte used was a 0.1 M solution of tetrabutyl ammonium hexafluorophosphate (TBAH) in UV-grade acetonitrile. The working electrode was a platinum disk and the auxiliary electrode was a platinum wire. Ag/AgCl was used as a reference electrode and was calibrated against the ferrocene/ferrocenium ($FeCp_2/FeCp_2^+$) redox couple as an internal standard (0.43 V vs. SCE) [15]. The cyclic voltammograms were obtained at a scan rate of 100 mV/s. All electrochemical data were collected for the complexes using the same electrodes and instrument settings to allow for observation of small changes in redox potentials.

2.7. Mass spectroscopy

The electrospray ionization mass spectra were measured using an Agilent Technologies 6220 Accurate-Mass TOF LC–MS with a dual ESI source. The solvent used was HPLC grade acetonitrile.

2.8. Photochemistry

Photocatalytic hydrogen production experiments were performed using previously reported conditions [11]. The acetonitrile,

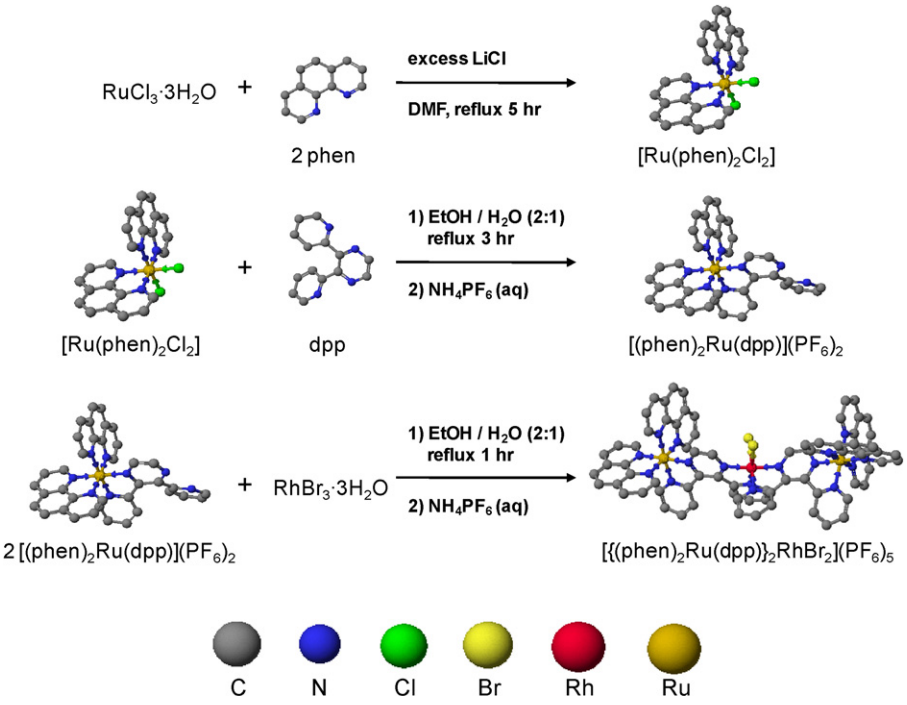

Scheme 1. Synthetic approach displaying the building block method of polyazine bridged, mixed-metal supramolecular complexes.

trimetallic complex, and water solution was degassed in the photolysis reaction cells using argon gas and were capped with air tight septa. The DMA was degassed separately and added to the reaction cells just prior to photolysis (final solution = 4.46 mL; 65 mM trimetallic complex, 1.5 M DMA, 0.62 M water acidified to pH = 2 using triflic acid, overall effective pH ~ 9.1). The samples were photolyzed from the bottom of the cells using a 470 nm LED light source array (each LED adjusted to 2 W output) which was constructed in our laboratory [16]. After 2 h of photolysis, a 100 μL sample of the reaction cell's headspace was injected into a series 580 GOW-MAC gas chromatograph, equipped with a rhenium–tungsten thermal conductivity detector and a 5 Å molecular sieves column using ultra-high purity argon gas, to analyze the amount of hydrogen produced. The signal was amplified with a Vernier Software instrument amplifier and recorded using Logger Pro 3.4.5 software. The gas chromatograph was calibrated for hydrogen signal sensitivity by injecting known amounts of hydrogen gas and generating a calibration curve. The total amount of hydrogen produced in the photolysis experiment was calculated by the summation of hydrogen in the headspace (from calibration curve) and hydrogen in the solution (Henry's Law) [17]. The reported value for hydrogen production is the average of three experiments performed.

3. Results and discussion

3.1. Synthesis

The dpp bridged Ru,Rh,Ru trimetallic complex $[\{(phen)_2Ru(dpp)\}_2RhBr_2](PF_6)_5$ was prepared following our building block synthetic approach. A schematic representation of the complete synthesis is detailed in Scheme 1. Initially, the phen terminal ligand was reacted with $RuCl_3{\cdot}3H_2O$ in DMF to obtain the $[(phen)_2RuCl_2]$ precursor [12]. The monometallic complex $[(phen)_2Ru(dpp)](PF_6)_2$ was prepared by reacting $[(phen)_2RuCl_2]$ in the presence of excess dpp, followed by purification on adsorption alumina. The complex $[\{(phen)_2Ru(dpp)\}_2RhBr_2](PF_6)_5$ was prepared by attaching two equivalents of the monometallic $[(phen)_2Ru(dpp)](PF_6)_2$ to a rhodium center by reacting with $RhBr_3{\cdot}3H_2O$. The complex $[\{(phen)_2Ru(dpp)\}_2RhBr_2](PF_6)_5$ was purified by recrystallization from hot ethanol and characterized by ESI-MS, electronic absorption spectroscopy, emission spectroscopy, electrochemical methods, and further used for the production of hydrogen from water in the presence of an electron donor.

3.2. Electrochemistry

The polyazine metal complexes show rich electrochemistry and the analysis of the electrochemical features gives insight into the orbital energetics of the various complexes. The cyclic voltammogram of $[\{(phen)_2Ru(dpp)\}_2RhBr_2](PF_6)_5$ is shown in Fig. 2. The redox potentials of the monometallic $[(phen)_2Ru(dpp)](PF_6)_2$, dpp ligand bridged bimetallic $[\{(phen)_2Ru\}_2(dpp)](PF_6)_4$, dpp ligand bridged heterotrimetallic $[\{(phen)_2Ru(dpp)\}_2RhBr_2](PF_6)_5$, and the corresponding relevant heterotrimetallic complexes reported are shown in Table 1. All of the complexes were studied simultaneously with the same electrodes, internal standards and instrument settings to allow for careful comparisons. The $Ru^{II/III}$ redox couple appears at +1.45 V for monometallic complex $[(phen)_2Ru(dpp)](PF_6)_2$. A positive shift in the oxidation of the ruthenium metal center ($Ru^{II/III}$) is observed as the number of metal

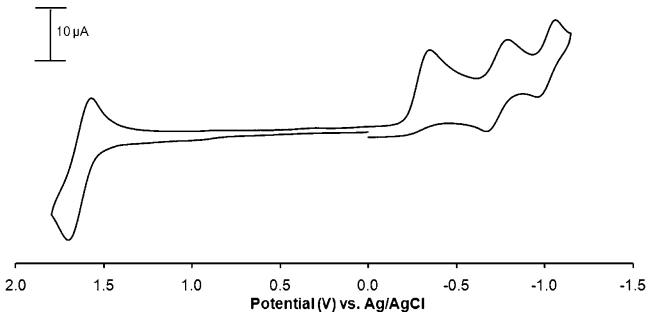

Fig. 2. Cyclic voltammogram of $[\{(phen)_2Ru(dpp)\}_2RhBr_2](PF_6)_5$ in 0.1 M TBAH in CH_3CN.

Table 1
Summary of electrochemical data.

Complex[a]	$E_{1/2}$ (V)	Assignments
$[(phen)_2Ru(dpp)](PF_6)_2$	+1.45	$Ru^{II/III}$
	−1.02	$dpp^{0/-}$
	−1.42	$phen^{0/-}$
$[\{(phen)_2Ru\}_2(dpp)](PF_6)_4$	+1.50	$Ru^{II/III}$
	+1.69	$Ru^{II/III}$
	−0.62	$dpp^{0/-}$
	−1.12	$dpp^{-/2-}$
	−1.41	$phen^{0/-}$
$[\{(bpy)_2Ru(dpp)\}_2RhCl_2](PF_6)_5$	+1.61[b]	$2Ru^{II/III}$
	−0.35[c]	$Rh^{III/II/I}$
	−0.76	$dpp^{0/-}$
	−1.01	$dpp^{0/-}$
$[\{(bpy)_2Ru(dpp)\}_2RhBr_2](PF_6)_5$	+1.61[b]	$2Ru^{II/III}$
	−0.32[c]	$Rh^{III/II/I}$
	−0.71	$dpp^{0/-}$
	−1.01	$dpp^{0/-}$
$[\{(phen)_2Ru(dpp)\}_2RhCl_2](PF_6)_5$	+1.61[b]	$2Ru^{II/III}$
	−0.35[c]	$Rh^{III/II/I}$
	−0.75	$dpp^{0/-}$
	−1.02	$dpp^{0/-}$
$[\{(phen)_2Ru(dpp)\}_2RhBr_2](PF_6)_5$	+1.62[b]	$2Ru^{II/III}$
	−0.32[c]	$Rh^{III/II/I}$
	−0.71	$dpp^{0/-}$
	−1.01	$dpp^{0/-}$

[a] Measured using Ag/AgCl reference electrode and 0.1 M Bu_4NPF_6 in acetonitrile as the supporting electrolyte.
[b] Two overlapping, reversible one-electron waves.
[c] Reported E_p^c of irreversible process.

centers increased. Coordination of the two $(phen)_2Ru^{II}$ subunits through the bridging ligand dpp shows a small positive shift in the oxidation potential described as lowering the energy of the Ru(dπ) orbitals, making the system more difficult to oxidize. The dpp ligand bridged Ru,Ru bimetallic complex $[\{(phen)_2Ru\}_2(dpp)](PF_6)_4$ shows two distinct $Ru^{II/III}$ oxidation events at +1.50 V and +1.69 V, indicating coupling of the metals in the bimetallic system. The trimetallic complexes $[\{(phen)_2Ru(dpp)\}_2RhCl_2](PF_6)_5$ and $[\{(phen)_2Ru(dpp)\}_2RhBr_2](PF_6)_5$ display two overlapping, one-electron oxidations around +1.61 V, indicating minimal electronic communication between the two ruthenium subunits in this motif. Coupling the rhodium to the dpp bridging ligand makes it more difficult to oxidize the ruthenium center in the trimetallic complexes compared to the mono- and bimetallic complexes.

The reductive side of the voltammogram of the supramolecular complexes displays ligand-based, as well metal-based, reductions. Reduction of the bridging ligand is observed first

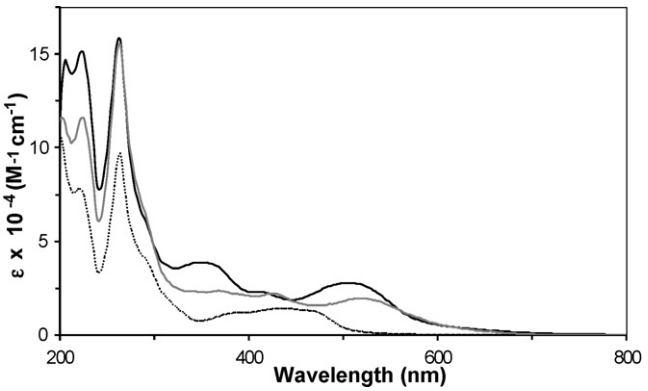

Fig. 3. Electronic absorption spectra of $[(phen)_2Ru(dpp)](PF_6)_2$ (····), $[\{(phen)_2Ru\}_2(dpp)](PF_6)_4$ (▬ ▬) and $[\{(phen)_2Ru(dpp)\}_2RhBr_2](PF_6)_5$ (– –) in CH_3CN at 298 K.

for the monometallic and bimetallic complexes representing the $dpp^{0/-}$ couple, illustrative of the low-lying π* orbital on the bridging ligand. Reduction of the terminal ligands occurs at more negative potentials. For $[(phen)_2Ru(dpp)](PF_6)_2$ and $[\{(phen)_2Ru\}_2(dpp)](PF_6)_4$, the LUMO is dpp(π*) based. In the Rh-containing trimetallic complexes, for example $[\{(phen)_2Ru(dpp)\}_2RhBr_2](PF_6)_5$, the first reduction occurs at −0.32 V (vs. Ag/AgCl reference) and is an irreversible reduction of the central $Rh^{III/II/I}$. The irreversible nature of the Rh reduction in these trimetallic complexes compare well with the previously described $[Rh(bpy)_2Cl_2]^+$ reduction with subsequent halide loss [18]. At more negative potentials there are two reversible dpp ligand-based reductions at −0.71 V and −1.01 V. Rh is reduced prior to the dpp ligands indicating that the trimetallic complex $[\{(phen)_2Ru(dpp)\}_2RhBr_2](PF_6)_5$ possess a Rh(dσ*) centered LUMO with energetically close dpp(π*) orbitals.

When comparing the Cl^- and Br^- containing trimetallics, a positive shift in the reduction of the Rh metal center is observed for the Br^- complexes. The trimetallic complexes $[\{(phen)_2Ru(dpp)\}_2RhBr_2](PF_6)_5$ and $[\{(bpy)_2Ru(dpp)\}_2RhBr_2](PF_6)_5$ display the $Rh^{III/II/I}$ irreversible reductions about 30 mV more positive than the corresponding chloride analogues $[\{(phen)_2Ru(dpp)\}_2RhCl_2](PF_6)_5$ and $[\{(bpy)_2Ru(dpp)\}_2RhCl_2](PF_6)_5$, indicating that the choice of halide ligand on the Rh metal center affects the orbital energetics of these trimetallic complexes. A similar pattern in the Rh reduction can be observed in the series of $[Rh(bpy)_2X_2]^+$ complexes (where X = Cl, Br, I) [19]. In the $[\{(phen)_2Ru(dpp)\}_2RhBr_2](PF_6)_5$ complex, the $Rh^{III/II/I}$ reduction shifts to more positive potential and can be attributed to the decrease in σ-donor ability of Br^- vs. Cl^-.

Table 2
Electronic absorption spectra summary.

Complex[a]	λ^{abs} (nm)	ε (10^{-4} M^{-1} cm^{-1})	Assignment
$[(phen)_2Ru(dpp)](PF_6)_2$[b]	465	1.39	Ru(dπ) → dpp(π*) CT
$[\{(phen)_2Ru\}_2(dpp)](PF_6)_4$[b]	526	2.34	Ru(dπ) → dpp(π*) CT
$[\{(bpy)_2Ru(dpp)\}_2RhCl_2](PF_6)_5$[c]	520	2.6	Ru(dπ) → dpp(π*) CT
$[\{(bpy)_2Ru(dpp)\}_2RhBr_2](PF_6)_5$[c]	520	2.6	Ru(dπ) → dpp(π*) CT
$[\{(phen)_2Ru(dpp)\}_2RhCl_2](PF_6)_5$[c]	520	2.6	Ru(dπ) → dpp(π*) CT
$[\{(phen)_2Ru(dpp)\}_2RhBr_2](PF_6)_5$	262	15.9	phen π → π*
	346	3.9	dpp π → π*
	418	2.3	Ru(dπ) → phen(π*) CT
	520	2.6	Ru(dπ) → dpp(π*) CT

[a] Measured in CH_3CN at room temperature.
[b] Ref. [20].
[c] Ref. [11].

3.3. Electronic absorption spectroscopy

The polyazine complexes are efficient light absorbers throughout the ultraviolet and visible regions. The electronic absorption spectra of $[(phen)_2Ru(dpp)](PF_6)_2$, $[\{(phen)_2Ru\}_2(dpp)](PF_6)_4$ and $[\{(phen)_2Ru(dpp)\}_2RhBr_2](PF_6)_5$ are shown in Fig. 3 and tabulated in Table 2. The complexes containing phen as the terminal ligand display phen-based internal ligand (IL) $\pi \rightarrow \pi^*$ transitions at 262 nm [20]. The energy of phen-based $\pi \rightarrow \pi^*$ transitions appear to be unaffected by coordination of multiple metal centers. The bridging ligand dpp-based $\pi \rightarrow \pi^*$ transitions display a bathochromic shift going from monometallic complex $[(phen)_2Ru(dpp)](PF_6)_2$ (292 nm) to the trimetallic complex $[\{(phen)_2Ru(dpp)\}_2RhBr_2](PF_6)_5$ (~346 nm). This is characteristic of the further stabilization of the dpp π^* acceptor orbital upon coordination to a second metal center.

In Ru–polyazine complexes, the visible region of the spectrum contains MLCT transitions that are $Ru(d\pi) \rightarrow L(\pi^*)$ in nature. The title complex possesses both $Ru(d\pi) \rightarrow phen(\pi^*)$ CT and $Ru(d\pi) \rightarrow dpp(\pi^*)$ CT transitions [11,13,20–22]. In these phen complexes, the higher energy CT transition has been assigned to the $Ru(d\pi) \rightarrow phen(\pi^*)$ CT and the lower energy CT transition assigned to the $Ru(d\pi) \rightarrow dpp(\pi^*)$ CT, consistent with the electrochemistry. Coordination of a second metal center (Ru or Rh) to the dpp bridging ligand decreases the energy of the $Ru(d\pi) \rightarrow dpp(\pi^*)$ CT transition in both the bimetallic and trimetallic motifs.

When comparing the complexes $[\{(phen)_2Ru(dpp)\}_2RhCl_2](PF_6)_5$ and $[\{(phen)_2Ru(dpp)\}_2RhBr_2](PF_6)_5$, variation of the halide ligand attached to the rhodium metal center appears to not exhibit a large difference in their optical properties. The light absorbing properties of $[\{(phen)_2Ru(dpp)\}_2RhCl_2](PF_6)_5$ and $[\{(phen)_2Ru(dpp)\}_2RhBr_2](PF_6)_5$ are almost identical in the UV and visible, consistent with the same light absorbing subunits.

3.4. Excited state properties

The excited state properties of the ^{3}MLCT state of all four Ru,Rh,Ru complexes have been simultaneously examined using emission spectroscopy and lifetime measurements and tabulated in Table 3. The emission profiles of $[(phen)_2Ru(dpp)](PF_6)_2$, $[\{(phen)_2Ru\}_2(dpp)](PF_6)_4$ and $[\{(phen)_2Ru(dpp)\}_2RhBr_2](PF_6)_5$ were measured at room temperature and 77 K, shown in Fig. 4, for a visual comparison. Upon photoexcitation from the ^{1}GS to the ^{1}MLCT excited state, the complex undergoes intersystem crossing to populate the emissive ^{3}MLCT excited state. The energy of the ^{3}MLCT emission, both at room temperature and 77 K, decreases from monometallic to multi-metallic complexes, as is paralleled with the $Ru(d\pi) \rightarrow dpp(\pi^*)$ MLCT transition in the electronic absorption spectra [23,24]. The 77 K emission profiles in Fig. 4 are blue-shifted with respect to the room temperature measurements. These emission profiles also display a poorly resolved vibrational progression indicating that no single vibrational mode dictates deactivation of the populated ^{3}MLCT excited state to the ^{1}GS [24].

Table 3
Photophysical properties of Ru,Rh,Ru complexes and related systems.

Complex[a]	λ^{em} (nm)[b]	Φ^{em} ($\times 10^2$)	τ (ns)
$[(bpy)_2Ru(dpp)](PF_6)_2$	682[c]	1.2	382[c]
$[(phen)_2Ru(dpp)](PF_6)_2$	668 (661[c])	2.7	460[c]
$[\{(bpy)_2Ru\}_2(dpp)](PF_6)_4$	790[c]	0.097	140[c]
$[\{(phen)_2Ru\}_2(dpp)](PF_6)_4$	750 (746[c])	0.16	153[c]
$[\{(bpy)_2Ru(dpp)\}_2RhCl_2](PF_6)_5$	776	0.026	38
$[\{(bpy)_2Ru(dpp)\}_2RhBr_2](PF_6)_5$	776	0.014	34
$[\{(phen)_2Ru(dpp)\}_2RhCl_2](PF_6)_5$	760	0.022	35
$[\{(phen)_2Ru(dpp)\}_2RhBr_2](PF_6)_5$	760	0.017	30

[a] In CH_3CN at room temperature.
[b] Emission spectra corrected for PMT response.
[c] Values from Ref. [20].

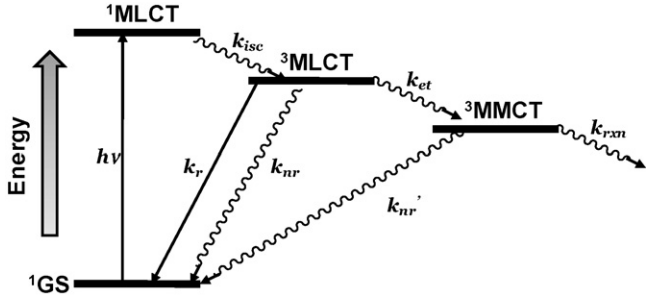

Fig. 5. Proposed energy state diagram of $[\{(phen)_2Ru(dpp)\}_2RhBr_2](PF_6)_5$. k_{isc} = intersystem crossing, k_r = radiative rate constant, k_{nr} = non-radiative rate constant, k_{et} = intramolecular electron transfer, and k_{rxn} = photochemical reaction.

Excited state properties similar to $[\{(bpy)_2Ru(dpp)\}_2RhCl_2](PF_6)_5$ and $[\{(bpy)_2Ru(dpp)\}_2RhBr_2](PF_6)_5$ are observed for the $[\{(phen)_2Ru(dpp)\}_2RhCl_2](PF_6)_5$ and $[\{(phen)_2Ru(dpp)\}_2RhBr_2](PF_6)_5$ trimetallic complexes. In these trimetallic complexes, incorporation of a rhodium center introduces metal-based low-lying $d\sigma^*$ acceptor orbitals which facilitates the electron transfer to ultimately form a metal-to-metal charge transfer (^{3}MMCT) excited state, Fig. 5. The quantum yield of emission from the ^{3}MLCT state in the trimetallic complexes is greatly reduced due to intramolecular electron transfer to populate the lower lying ^{3}MMCT excited state. In comparison to the $[\{(phen)_2Ru\}_2(dpp)](PF_6)_4$ bimetallic model system ($\lambda^{em} = 750$ nm, $\Phi^{em} = 1.6 \times 10^{-3}$), $[\{(phen)_2Ru(dpp)\}_2RhCl_2](PF_6)_5$ and $[\{(phen)_2Ru(dpp)\}_2RhBr_2](PF_6)_5$ show a decrease in emission quantum yield ($\Phi^{em} = 2.2 \times 10^{-4}$ and 1.7×10^{-4}, respectively).

The $Ru(d\pi) \rightarrow Rh(d\sigma^*)$ ^{3}MMCT excited state depopulates through either radiative or non-radiative relaxation to the ^{1}GS or an excited state reaction. Coupling with a decrease in emission quantum yield in this trimetallic form, there is an associated decrease in the excited state lifetime of $[\{(phen)_2Ru(dpp)\}_2RhCl_2](PF_6)_5$ and $[\{(phen)_2Ru(dpp)\}_2RhBr_2](PF_6)_5$ trimetallic complexes (35 ns and

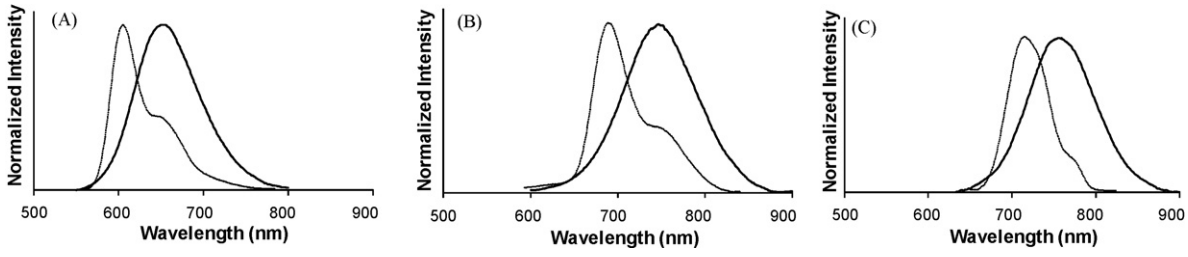

Fig. 4. Emission profiles of $[(phen)_2Ru(dpp)](PF_6)_2$ (A), $[\{(phen)_2Ru\}_2(dpp)](PF_6)_4$ (B) and $[\{(phen)_2Ru(dpp)\}_2RhBr_2](PF_6)_5$ (C) at room temperature (—) and 77K (▬).

Table 4
Photocatalytic hydrogen production.

Complex[a]	H_2 (μmol)	Turnovers
$[\{(bpy)_2Ru(dpp)\}_2RhCl_2](PF_6)_5$[b]	6.0 ± 0.7	22
$[\{(bpy)_2Ru(dpp)\}_2RhBr_2](PF_6)_5$[b]	7.2 ± 0.8	27
$[\{(phen)_2Ru(dpp)\}_2RhCl_2](PF_6)_5$[b]	5.4 ± 0.5	20
$[\{(phen)_2Ru(dpp)\}_2RhBr_2](PF_6)_5$	6.5 ± 0.2	24

[a] Values shown are after 2 h of photolysis using 470 nm LED light source.
[b] Ref. [11].

30 ns, respectively) compared to the $[\{(phen)_2Ru\}_2(dpp)](PF_6)_4$ bimetallic complex (153 ns). It is interesting to note that both the phen monometallic and bimetallic complexes with dpp-based ^{3}MLCT excited states display a larger emission quantum yield and excited state lifetime compared to their bpy analogues. In the trimetallic systems, the emission quantum yields and excited state lifetimes are similar with TL = phen or bpy. Altering the halide ligand does appear to influence the emission quantum yield as well as the lifetime of the ^{3}MLCT excited state. In both the bpy and phen trimetallic systems, variation of the halide from Cl^- to Br^- shows a decrease in the ^{3}MLCT excited state emission quantum yield and lifetime. This observation indicates an increased rate of population of the ^{3}MMCT excited state and that halide variation on the rhodium metal does influence the photophysical properties of the trimetallic complexes. Despite the longer lived ^{3}MLCT state in $[(TL)_2Ru(dpp)]^{2+}$ and $[\{(TL)_2Ru\}_2(dpp)]^{4+}$ when TL = phen vs. bpy, the incorporation of phen into our Ru,Rh,Ru trimetallic complexes does not enhance the ^{3}MLCT excited state lifetime.

3.5. Photochemistry

Photolysis of dpp bridged Ru,Rh,Ru trimetallic complexes in an acetonitrile and water solution in the presence of an electron donor generates hydrogen gas. The complex $[\{(bpy)_2Ru(dpp)\}_2RhCl_2](PF_6)_5$ is the first photochemical molecular device shown to act as a photoinitiated electron collector at a reactive metal center that stays intact after reducing water to produce hydrogen in the presence of N,N-dimethylaniline (DMA). Photoinitiated electron collection by $[\{(bpy)_2Ru(dpp)\}_2Rh^{III}Cl_2]^{5+}$ undergoes reduction of the electron collecting Rh^{III} center to form Rh^I, followed by halide loss to yield the square planar Rh^I species $[\{(bpy)_2Ru(dpp)\}_2Rh^I]^{5+}$. Substitution of chloride by bromide in $[\{(bpy)_2Ru(dpp)\}_2RhX_2]^{5+}$ (where X = Cl or Br), has shown enhanced photocatalytic hydrogen production from water, Table 4. The complexes $[\{(bpy)_2Ru(dpp)\}_2RhCl_2](PF_6)_5$ and $[\{(bpy)_2Ru(dpp)\}_2RhBr_2](PF_6)_5$ produced 6.0 μmol and 7.2 μmol of hydrogen, respectively, in 2 h upon photolysis with a 470 nm LED in the presence of DMA. This enhanced photocatalytic activity has been attributed to the increased ease of halide loss or increased rate of electron transfer. The photochemical molecular device is tunable by modification of the terminal ligand, bridging ligand and/or halide to obtain further insight into the photocatalytic mechanisms involved in the production of hydrogen gas.

Varying the terminal ligand from bpy to phen generated new photoinitiated electron collectors, $[\{(phen)_2Ru(dpp)\}_2RhCl_2](PF_6)_5$ and $[\{(phen)_2Ru(dpp)\}_2RhBr_2](PF_6)_5$, which can photocatalytically reduce water to hydrogen gas. The spectroscopic, electrochemical and photophysical properties of the terminal ligand modified complexes $[\{(phen)_2Ru(dpp)\}_2RhX_2](PF_6)_5$ (where X = Cl or Br) resemble the initial complexes studied $[\{(bpy)_2Ru(dpp)\}_2RhX_2](PF_6)_5$ despite the longer lived ^{3}MLCT excited states of the phen vs. bpy monometallic synthons. The complexes $[\{(phen)_2Ru(dpp)\}_2RhCl_2](PF_6)_5$ and $[\{(phen)_2Ru(dpp)\}_2RhBr_2](PF_6)_5$ photochemically produced 5.4 μmol and 6.5 μmol of H_2 gas, respectively, in 2 h in the presence of DMA. The bromide complex is slightly more active than the corresponding chloride complex. This observation once again confirms the concept that during photoinitiated electron collection, the electron collecting Rh^{III} center reductively loses the bound halides to form a catalytically activated Rh^I species which can then reduce water into hydrogen. The phen complexes consistently produce lower amounts of H_2 than their bpy analogues. This is surprising given the longer lived ^{3}MLCT excited states of the related phen vs. bpy monometallic and bimetallic complexes.

4. Conclusions

The supramolecular complex $[\{(phen)_2Ru(dpp)\}_2RhBr_2](PF_6)_5$ has been developed by component modification of our original Ru,Rh,Ru trimetallic complex, $[\{(bpy)_2Ru(dpp)\}_2RhCl_2](PF_6)_5$, through terminal ligand variation at the light absorber Ru center and halide variation at the electron collector Rh reactive center. The electrochemical properties of $[\{(phen)_2Ru(dpp)\}_2RhBr_2](PF_6)_5$ show that the Rh reduces prior to the dpp bridging ligand supporting the conclusion of a Rh-based LUMO. The spectroscopic and photophysical properties display population of the emissive ^{3}MLCT excited state followed by intramolecular electron transfer to populate the ^{3}MMCT excited state. The ability of the $[\{(phen)_2Ru(dpp)\}_2RhBr_2](PF_6)_5$ trimetallic complex to photocatalytically generate hydrogen in the presence of a sacrificial electron donor and water has been observed. Enhancement in the production of H_2 was observed for the $[\{(phen)_2Ru(dpp)\}_2RhBr_2](PF_6)_5$ compared to $[\{(phen)_2Ru(dpp)\}_2RhCl_2](PF_6)_5$, with the same trend observed for the bpy terminal ligand analogues $[\{(bpy)_2Ru(dpp)\}_2RhBr_2](PF_6)_5$ and $[\{(bpy)_2Ru(dpp)\}_2RhCl_2](PF_6)_5$. The decrease in the σ donating ability of Br^- vs. Cl^- appears to have an effect on the photocatalytic properties of these Ru,Rh,Ru trimetallic complexes as both $[\{(phen)_2Ru(dpp)\}_2RhBr_2](PF_6)_5$ and $[\{(bpy)_2Ru(dpp)\}_2RhBr_2](PF_6)_5$ generate more H_2 than their respective Cl^- analogues. Current studies involve further variation of the terminal ligand to investigate the impact this has on the spectroscopic, photophysical, electrochemical and photochemical properties and a more detailed mechanistic study of the photocatalysis process.

Acknowledgements

Acknowledgment is made to the Chemical Sciences, Geosciences and Biosciences Division, Office of Basic Energy Sciences, Office of Sciences, U.S. Department of Energy for their generous financial support of this research. Acknowledgment is also made to the financial collaboration of Phoenix Canada Oil Company, which holds long-term license rights to commercialize the technology.

References

[1] V. Balzani, L. Moggi, F. Scandola, Supramolecular photochemistry NATO ASI Series, vol. 214, Reidel, Dordrecht, 1987, p. 1.
[2] V. Balzani, A. Juris, M. Venturi, Chem. Rev. 96 (1996) 759.
[3] M.T. Indelli, C. Chiorboli, F. Scandola, Topics in Current Chemistry, Springer, Verlag, 2007, p. 215.
[4] R. Konduri, H. Ye, F.M. MacDonnell, S. Serroni, S. Campagna, K. Rajeshwar, Angew. Chem. Int. Ed. 41 (2002) 3185.
[5] S.M. Molnar, G.E. Jensen, L.M. Volger, S.W. Jones, L. Laverman, J.S. Bridgewater, M.M. Richter, K.J. Brewer, J. Photochem. Photobiol. A: Chem. 80 (1994) 315.
[6] S.M. Molnar, G. Nallas, J.S. Bridgewater, K.J. Brewer, J. Am. Chem. Soc. 116 (1994) 5206.
[7] C. Chiorboli, S. Fracasso, M. Ravaglia, F. Scandola, S. Campagna, K.L. Wouters, R. Konduri, F.M. MacDonnell, Inorg. Chem. 44 (2005) 8368.
[8] M. Kim, R. Konduri, H. Ye, F.M. MacDonnell, F. Puntoriero, S. Serroni, S. Campagna, T. Holder, G. Kinsel, K. Rajeshwar, Inorg. Chem. 41 (2002) 2471.
[9] M. Elvington, K.J. Brewer, Inorg. Chem. 45 (2006) 5242.

[10] S.M. Arachchige, J. Brown, K.J. Brewer, J. Photochem. Photobiol. A: Chem. 197 (2008) 13.
[11] S.M. Arachchige, J. Brown, R.E. Chang, A. Jain, D.F. Zigler, K. Rangan, K.J. Brewer, Inorg. Chem. 48 (2009) 1989.
[12] B.P. Sullivan, D.J. Salmon, T.J. Meyer, Inorg. Chem. 17 (1978) 3334.
[13] A.W. Wallace, W.R. Murphy, J.D. Petersen, Inorg. Chim. Acta 166 (1989) 47.
[14] J.V. Caspar, E.M. Kober, B.P. Sullivan, T.J. Meyer, J. Am. Chem. Soc. (1982) 630.
[15] T. Gennett, D.F. Milner, M.J. Weaver, J. Phys. Chem. 89 (1985) 2787.
[16] J. Brown, R.M. Elvington, M.T. Mongelli, D.F. Zigler, K.J. Brewer, Proc. SPIE 6340 (2006) 634007W1.
[17] Purwanto, R.M. Deshpande, R.V. Chaudhari, H. Delmas, J. Chem. Eng. Data 41 (1996) 1414.
[18] G. Kew, K. DeArmond, K. Hanck, J. Phys. Chem. 78 (1974) 727.
[19] D. Amarante, C. Cherian, C. Emmel, H. Chen, S. Dayal, M. Koshy, E. Megehee, Inorg. Chim. Acta 358 (2005) 2231.
[20] K. Kalyanasundaram, M.K. Nazeeruddin, Inorg. Chem. 29 (1989) 1888.
[21] K. Kalyanasundaram, M. Gratzel, M.K. Nazeeruddin, J. Phys. Chem. 96 (1992) 5865.
[22] W.R. Murphy, K.J. Brewer, G. Gettliffe, J.D. Petersen, Inorg. Chem. 28 (1989) 81.
[23] C.H. Braunstein, A.D. Baker, T.C. Strekas, H.D. Gafney, Inorg. Chem. 23 (1984) 857.
[24] Y. Fuchs, S. Lofters, T. Dieter, W. Shi, R. Morgan, T.C. Strekas, H.D. Gafney, A.D. Baker, J. Am. Chem. Soc. 109 (1987) 2691.